Materials & Design 83 (2015) 276–283

Contents lists available at ScienceDirect

Materials & Design

journal homepage: www.elsevier.com/locate/matdes

Simplified fractal FEA model for the estimation of the Young's modulus of Ti foams obtained by powder metallurgy

L. Pérez [a], S. Lascano [b], C. Aguilar [c], D. Domancic [b], I. Alfonso [d,*]

[a] Department of Mechanical Engineering, Advanced Center for Electrical and Electronic Engineering (Basal Project FB0008), Universidad Técnica Federico Santa María, Av. España 1680, Casilla 110-V, Valparaíso, Chile
[b] Department of Mechanical Engineering, Universidad Técnica Federico Santa María, Av. España 1680, Casilla 110-V, Valparaíso, Chile
[c] Departamento de Ingeniería Metalúrgica y Materiales, Universidad Técnica Federico Santa María, Av. España 1680, Casilla 110-V, Valparaíso, Chile
[d] Instituto de Investigaciones en Materiales, Unidad Morelia, Universidad Nacional Autónoma de México, Campus Morelia UNAM, Antigua Carretera a Pátzcuaro No. 8701, Col. Ex-Hacienda de San José de la Huerta, CP. 58190 Morelia, Michoacán, Mexico

ARTICLE INFO

Article history:
Received 27 February 2015
Revised 28 May 2015
Accepted 6 June 2015
Available online 19 June 2015

Keywords:
Foam
Fractal
FEA
Model
Powder metallurgy
Ti

ABSTRACT

This work reports the introduction of a new finite elements model, for the estimation of the Young's modulus (E) of metallic foams obtained by means of powder metallurgy using a Space Holder Phase (SHP). The model is based on the reduction of the volume, and the replication of the expected porosity distribution as fractal using two different pore sizes, which depend on the SHP. Ti foams with porosities ranging from 30% to 70% were experimentally obtained and characterized to validate the model. The effect of the porosity on the Young's modulus for the Ti foams was estimated using the proposed model, and compared to the experimental values. Estimations obtained were in excellent agreement with the experimental results, with relative errors ranging from 0.8% to 11.2%. Both, experimental and estimated values for E showed important decreases as the porosity increases: e.g. E estimations were 37.1 and 9.3 GPa for porosities of 30% and 70%, respectively. The results demonstrated the fractal behavior of the porosity for the experimental metallic foams, as well as the efficacy of the proposed model for predicting the mechanical properties of these materials, being an important tool for their design and manufacture.

1. Introduction

The importance of the metallic foams has increased due to their unique combination of properties derived from their structures [1], presenting exceptional mechanical, thermal, acoustic, electrical and chemical properties [2–4], being used in a wide range of structural and functional products. These materials can be manufactured by a wide variety of methods, and among the most important are those that involve the incorporation of a removable Space Holder Phase (SHP). Two of the most used methods that include SHP are the infiltration of liquid metal, and conventional powder metallurgy (PM) [5,6]. PM process includes the Sintering and Dissolution Process (SDP), used to date to obtain foams of different materials (e.g. Al, Cu, Mg and Ti) with good mechanical properties and interconnected pores [7–9]. It has been found that depending on the SHP size and morphology, the pores network changes, being or not homogeneous their sizes and shapes, so it is very important the SHP selection because it controls the porosity. For Ti foams, different SHP have been used, such as NaCl, naphthalene, saccharose, KBr, and NH_4HCO_3 [9–13]. For the specific case of the NaCl, different studies have been made including design, processing and characterization [14,15]. It is important to remark that among the most important properties to be determined for Ti foams (mainly for biomedical applications) is the elastic modulus. The interest in the study of this parameter is due to the effect called stress-shielding, originated by the mismatch between the elastic moduli of Ti implants and human bones (110 and around 1–30 GPa, respectively). The Ti-based metallic foams are attractive because it is possible to modify their elastic modulus and decrease the stress-shielding [13–15]. Then, for the analysis of new foams it is very important to predict their mechanical behavior, besides the effect of the SHP and the manufacture process on these properties. One of the methods used to predict foams properties is the Finite Element Analysis (FEA), very useful to analyze foams due to its modeling capability, being able to model different geometries and their effect on the mechanical properties [16]. For foam models, the validity of the estimations mostly depends on the proximity of the model to the real foam topology. This fact has led to investigate new models and modifications to existing models, in

* Corresponding author.
E-mail address: ialfonso@unam.mx (I. Alfonso).

http://dx.doi.org/10.1016/j.matdes.2015.06.038
0264-1275/

order to obtain estimations in better agreement with the experimental results than those obtained using conventional models. Although the size distribution of the SHP is not always centralized, most of the works use only one pore size (usually the average size) in order to minimize the model complexity and the computer requirements [16,17]. Some works have used fractal approaches to study different metallic foams, for example using the "Sierpinski carpet" [18], or a fractal mesh model [19]. These works try to reduce the problems inherent to extract a representative cell for metallic foams, which are inherently disordered: non-equally sized and various shaped cells. Nevertheless, no works were found where Finite Elements (FE) models of metallic foams were obtained using this method. "Fractals" were proposed by Mandelbrot et al. [20], and it is a non-Euclidean geometry theory used to describe the irregularity in nature. There are different ways to define fractals: by dimension (e.g. by using the box-counting method), or by distribution (e.g. by a log–log frequency histogram of a certain feature). The use of the fractal dimension (D_f) has demonstrated that it is a very important tool to analyze the microstructure of different materials [21]. In the case of a porous fractal material, the relationship that must be satisfied is [20]:

$$Log(N_r) = -Df\ Log(r) \tag{1}$$

where N_r is the number of pores of a size r. For the determination of the dimension of the porous volume (D) using the pore distribution:

$$Log(V_r) = (3 - D)Log(r) \tag{2}$$

where V_r is the volume of the pores with a radius r, and the 3 is referred to the topological dimension of the pores volume.

In the case of porous materials, the fractal analysis has been widely used to analyze self-similarity at different scales, for example, porosity and microporosity in natural reservoirs [22]. The fractal analysis of metallic foams could be very useful due to the fact that changes in the porosity (size and volume fraction of pores) affect the D_f values. Besides, D_f can describe the heterogeneity or complexity of the system [23]. In the present work, our first objective is to introduce a new fractal FE model, dependent on the space holder particles used in the manufacturing process, in order to analyze the effect of the porosity on the elastic compressive behavior of metallic foams. Our second objective is to compare the predictions with the experimental results for Ti foams obtained by the SDP route. These objectives are focused to validate the model for obtaining a better approach to the real microstructure and a good porosity-properties correlation, a very important fact for the design and manufacture of these materials.

2. Experimental

2.1. Space holder particles

In this work, five Ti foams with porosities ranging from 30% to 70% were obtained using a space holder, by the SDP. This manufacturing process is the starting point to obtain a FE model closer to the real foams morphologies, because these materials are highly dependent on the sintering parameters, mainly the morphology of the space holder. The morphology of the Ti particles used for the foams manufacture (grade 4, ASTM F67 Standard, Se-Jong Materials Co. Ltd, 99.5% purity, average diameter of 25 ± 3 μm) can be observed in Fig. 1a [using a FE-SEM FEI Scanning Electron Microscope (SEM)]. The NaCl particles (Panreac Quimica Sau, 99.5% purity) used as space holder can be seen in Fig. 1b. The analysis of these particles showed that their size distribution is not normal, but presents fractal characteristics: a high quantity of small diameter particles compared to a lower quantity of bigger particles. In this specific case, particles with average and maximum

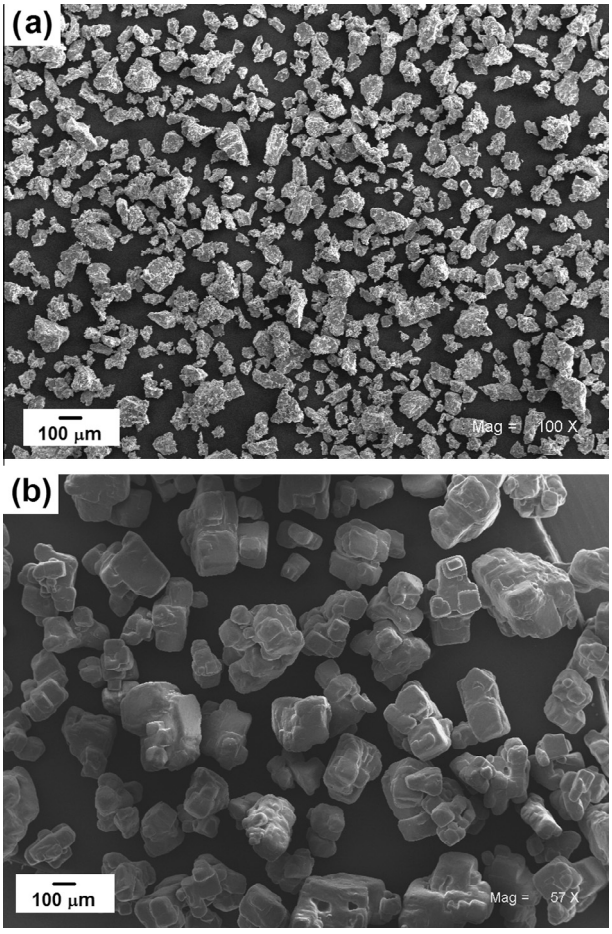

Fig. 1. SEM micrographs of: (a) Ti powder and (b) NaCl, used as SHP.

equivalent diameters of 420 ± 40 and 800 ± 65 μm, respectively, in an approximately 4:1 frequency ratio.

The equivalent diameter (D_e), used for the analysis of the particles size distribution, is defined as the diameter of a circle with equivalent area [24] and is given by Eq. (3):

$$D_e = \frac{1}{n}\sum\left(\frac{4A_p}{\pi}\right)^{1/2} \tag{3}$$

where A_p is the particle area, P_p its perimeter, and n the number of measured particles. The geometries of the particles were also analyzed using the shape factor (F). A perfect circle will have a shape factor of 1, while the shape factor of a line will approach to zero, and is defined in Eq. (4) [24]:

$$F = \frac{1}{n}\sum\left(\frac{4\pi A_p}{P_p^2}\right) \tag{4}$$

2.2. Foams manufacture

The powders (Ti + NaCl) were mixed for 40 min in order to obtain a good homogeneity, using the corrected proportions to obtain porosities of 30, 40, 50, 60 and 70 vol.%. The mixtures were introduced into a steel mold and uniaxially pressed to produce cylindrical compacts with 8 mm in diameter and 12 mm in length. The pressure used for the compaction stage was 800 MPa for all samples. The NaCl fraction of the obtained green compact was dissolved by immersion in a distilled water bath at 25 °C for 2 h, revealing the pores. Finally, the sintering process was carried out

at 1250 °C in vacuum (5×10^{-4} mbar) into a Carbolyte STF 15/75/450 furnace. These experimental parameters were defined according to the results of a previous work [15].

2.3. Foams characterization

The obtained foams were characterized using a Nikon Epiphot Optical Microscope (OM), and a Carl Zeiss EVO-MA10 SEM, to determinate the pore size and distribution. Total porosity, P_f, was also determined, through the following equation [25]:

$$P_f = \frac{(1-\rho_f)}{\rho_{Ti}} \tag{5}$$

where ρ_{Ti} is the Ti density and ρ_f is the foam density. NaCl and Ti densities are 2.17 and 4.51 g/cm^3, respectively. The densities of the foams were determined using the conventional equation for density (mass/volume), while the volumes were measured by the Archimedes principle. The geometries of the pores were analyzed using D_e and F through Eqs. (3) and (4), respectively. Young's moduli of the specimens, measured by means of compression tests, were conducted on an INSTRON 5505 materials testing machine, according to the ASTM E9 test. Specimens with height/diameter ratios of 0.8 were used (diameter 8 mm and height 6.4 mm) for this test.

3. Modeling and simulation

3.1. Models of the cylindrical sample

In order to estimate the Young's modulus of the foams, new FE models were used. These estimations were compared to the results obtained from the experiments in order to validate the models. The FE models used for the analysis of the Ti foams were chosen on the basics of the characteristics of the manufacturing process, mainly the morphology of the SHP. This is a critical parameter for obtaining a better prediction of the real microstructures, leading to estimations closer to the experimental results. A number of models have been developed for representing metallic foams, and many of them have been implemented in the commercial FE codes, from the use of only one unit cell [17], to the analysis of the complete foam [7,16,26]. In this work, we are introducing a new model, which consists on a cylindrical specimen with a central hole, used in order to decrease the computer requirements (use of less nodes and/or elements). The size of this hole must be selected so that the nominal diameter of the foam (solid wall) be wide enough to contain a significant quantity of unit cells or representative volume elements (RVE), for the convergence of the FEA results. Computations convergence have been analyzed in other works, founding that RVEs must be at least ~2.5–3.5 times the maximum size of certain feature that represents the material (unit cell) [27]. Considering this criterion, in our models the walls have four times the size of the unit cell. Besides, the size of these models was minimized compared to the size of the specimens used for experimental compression tests, in order to minimize computer requirements. This assumption can be made due to the fact that previous works [8,14,15] showed that the metallic foams present pores not only produced by the SHP, but also additional porosity associated to the sintering process (interparticle porosity). The total quantity of these small pores (generally with equivalent diameters between 5 and 20 μm) is much higher than the pores originated due to the SHP.

3.2. Fractal model for the porosity

If we assumed that the behavior of the total porosity for metallic foams is fractal, and we know the quantity of the pores originated by the SHP (depending on the porosity percentage), we could obtain the total and relative quantities of the smaller pores using a log–log plot according to Eq. (1) or Eq. (2). The porosity of the metallic foams could be modeled as a fractal taking into account: (i) the equivalent diameter distribution of the NaCl particles (a high quantity of particles with a size of ~400 μm and a low quantity of particles of ~800 μm); (ii) the fracture of the NaCl particles due to the applied pressure during the process, originating smaller particles; and (iii) the great quantity of small diameter pores produced in the sintering process (interparticle porosity) [7]. That is why the fractal models here proposed consider a low quantity of high diameter pores and a high quantity of smaller ones, in a ratio of $nr : 4n\frac{r}{2} : 16n\frac{r}{4}; \ldots; qn\frac{r}{p}$, where n is the total quantity and r is the diameter of the biggest pores ($q = p^2$). Then, the pores distribution could be modeled including at least two different pore sizes: the biggest of 800 μm and the intermediate ones of 400 μm, avoiding modeling the smallest pores considering the enormous quantity of them that would be included. Using as an example the foams with 30% of porosity, must be a total quantity of 240 pores of 800 μm, 960 pores of 400 μm (= 240 × 4), 384,000 of 20 μm and 1,536,000 of 10 μm (for 10 μm $p = 80$, and as $q = p^2$, then $q = 6400$), being 12.29 μm the average equivalent diameter. Taking into account the fractal approximation, we can replicate the fractal porosity in our model of reduced scale, only using pores of 10 and 20 μm in diameter, also in a ratio 4:1, and analyze the compressive behavior of the porous matrix. This approximation, using small pores and avoiding the use of the biggest ones, is possible due to fact that the average of the pores equivalent diameter, according to our models, is in the range of 10–20 μm due to the already shown high quantity of pores of small sizes (e.g. D_e average for the model of 30% of porosity was shown to be ~12 μm). Otherwise, the shape of the NaCl particles (see Fig. 1b), used as SHP in this work, is cubical with rounded edges, being aggregated in some cases. So, the pores could be modeled as spheres in order to avoid sharp edges and make easier the modeling process, supported by a previous work which showed that the use of this geometry for the pores delivers good estimations [7].

3.3. Finite elements model

The dimensions of the reduced representative volume element can be obtained using the ratio between the radii of the pores (spheres) and the cylinder, been 0.1. The defined dimensions of the reduced models were 0.20 mm in diameter and 0.16 mm in length (height/diameter ratios also = 0.8 for simulating the compression test), and a central hole of 0.08 mm in diameter. In order to probe the validity of the use of a central hole, a comparison was made between a model without any hole and models with holes ranging from 0.02 to 0.16 mm in diameter, for the foams with a porosity of 50%. It was found that for values from 0.02 to 0.08, the differences between the estimated Young's moduli (obtained with and without the hole) were lower than 3%, demonstrating the validity of the use of this model. For values up to 0.10, this difference exponentially increased, reaching ~50% for a hole with 0.16 mm in diameter, demonstrating that the size of the wall must be thick enough to contain a significant quantity of unit cells (as above mentioned, ~2.5–3.5 times the size of the unit cell). This analysis was also developed for models without pores, resulting in a linear behavior. Furthermore, the differences between the estimated Young's moduli obtained with and without the holes were lower than 6%, even for the holes with the highest diameters. ANSYS 15 FEA software was employed for modeling and theoretical calculations. The pores were modeled as a connected network for porosities of 50%, 60% and 70% (due to the high level of

porosity), while for 30% and 40% the relatively low porosity led to non-connected porosity models. Examples of the models are observed in Fig. 2a–c, for porosities of 30%, 50% and 70%. As can be observed, spherical pores with two different sizes were modeled according to the sizes of the NaCl particles already described (average and maximum sizes).

3.4. Simulation

Young's moduli of the metallic foams with different porosities were uni-axially estimated when applying equivalent compressive stresses of 20 MPa on the upper end nodes of the cylindrical specimens. The solid 187 3-D 10-node tetrahedral structural solid element was employed for meshing. This element is well suited to modeling irregular meshes, such as those produced for porous materials. Small elements were used to ensure the connectivity, as can be observed in Fig. 3a and b for the model of foams with 40% of porosity. Mesh convergence analysis was carried out by incrementally increasing the number of elements and verifying the estimations, to ensure convergence of the numerical solution. The final number of nodes used for the models was between 1×10^6 and 1.8×10^6, while the number of elements was between 0.6×10^6 and 1.2×10^6.

The coupled-node boundary condition (keeping the nodes in the same plane) was used for the upper face of the cylinder (see Fig. 3a). This condition is applied since the presence of pores causes un-even surfaces and making the deformation measurement hard to define. The nodes of the bottom were constrained for z displacement, while the movement of the surfaces of the internal hole was radially fixed. Young's modulus can be obtained from the response of the compression test, and along the z-axis (E_z) can be determined by:

$$E_z = \frac{\sigma_z}{\varepsilon_z} \tag{6}$$

where σ_z and ε_z are the stress and the strain in z-axis, respectively. The displacement of the cylinder in z-axis (u_z) is measured from the FEA estimations, and used for the strain determination:

$$\varepsilon_z = \frac{u_z}{L_z} \tag{7}$$

where L_z is the original height of the cylindrical specimen. Young's modulus (63 GPa) and Poisson Ratio (0.36) used for simulations were obtained from a specimen sintered without SHP, resulting in the absence of induced porosity. The simulated linearly elastic mechanical compressive testing was compared to experimental measurements of the Young's modulus. The analysis of the results will allow a better knowledge of the porosity and its effect on the mechanical behavior of the foams.

4. Results and discussion

4.1. Real and modeled foams porosities

Examples of the Ti foams with different porosities, obtained using the SDP route, are depicted in Fig. 4a–c. As can be seen, the foams are homogeneous and compact, while the porosities are well observed and homogeneously distributed. The real porosities, calculated using Eq. (5), were 28%, 38%, 47%, 58% and 68%, not exactly the expected values (30%, 40%, 50%, 60% and 70%), but very close to them. Obtained porosities are always lower than the nominal space-holder content, a consequence of two important facts: (i) a high compaction pressure implies a severe plastic deformation of the space-holder, which allows the coalescence between pores, and therefore, a higher interconnected porosity, and (ii) the metallic framework shrinkage during sintering, which generates a reduction in surface energy of particles [13]. The measured densities were 3.2, 2.7, 2.3, 1.9 and 1.5 g/cm^3, for the foams with porosities of 28%, 38%, 47%, 58% and 68%, respectively (4.51 g/cm^3 for pure Ti).

In order to analyze the mismatch between the models and the experimental foams, micrographs of the matrices at higher magnifications were obtained. Using these micrographs, the shape factors (F) were calculated using Eq. (4). The average shape factors for all the specimens are near 0.85, very close to a circle (a perfect circle will have a shape factor of 1), showing that the use of spheres in our model is not far from the real pores shape. Otherwise, the fractal dimensions (D_f) of these images were determined using the "box-counting" method. Fig. 5a–c shows a combination of OM micrographs and the proposed models for the foams with three porosities (30%, 50% and 70%). As can be observed, the foams exhibit both pore size and porosity distributions similar to the modeled ones. The biggest pores have average equivalent diameters of 780 ± 88 μm, corresponding to the NaCl particles size, the SHP. Besides, a high quantity of smaller pores can be observed, which have average D_e of 350 ± 39 μm. Interparticle pores expected to appear cannot be observed at this magnification, and will be further analyzed. The fractal dimensions in this figure reveal that real and modeled pore networks are very similar for each porosity percentage, demonstrating that match at different scales. Besides, D_f increases with the porosity increase, an expected result because D_f is a measure of a geometry complexity: greater the dimension, the more heterogeneous and complex the fractal object is. These results show that the modeled porosities matched to the real ones,

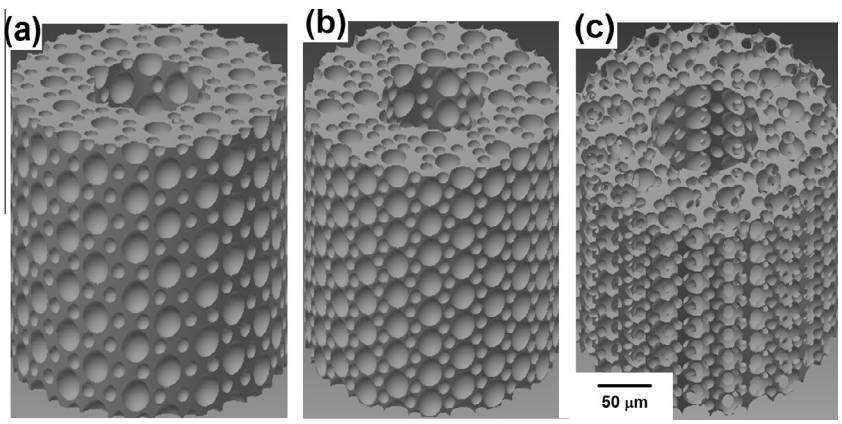

Fig. 2. Finite elements models using ANSYS, for the foams with porosities of: (a) 30%, (b) 50% and (c) 70%.

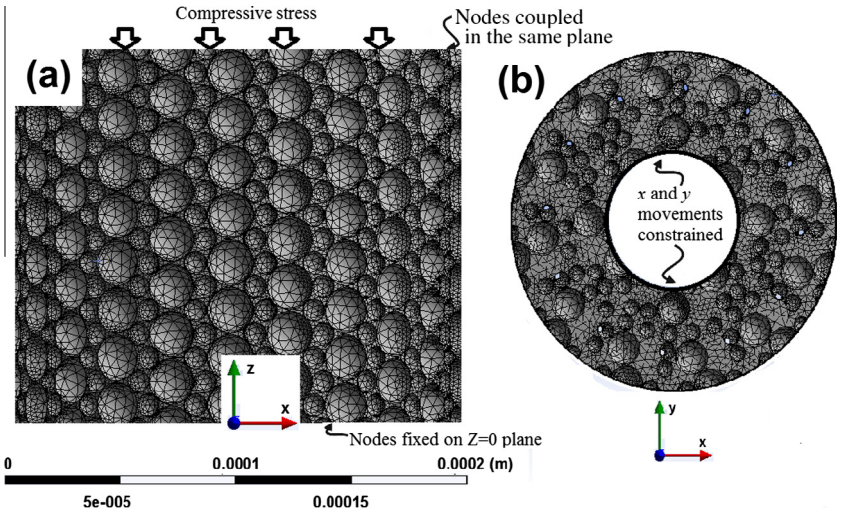

Fig. 3. Longitudinal (a) and axial (b) views of the meshed model of a Ti foam with a porosity of 40%.

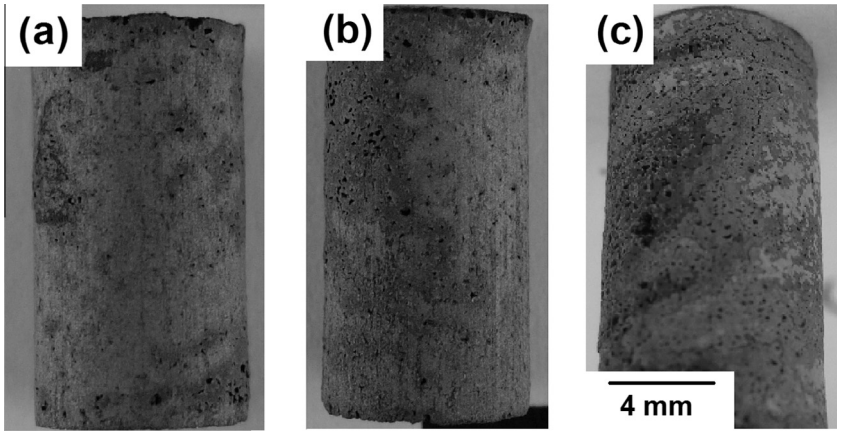

Fig. 4. Ti foams obtained using as SHP with porosities of: (a) 30%, (b) 50% and (c) 70%.

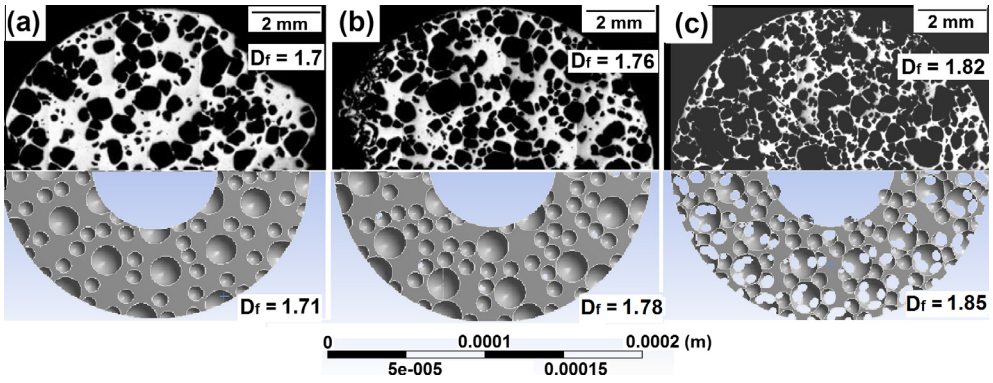

Fig. 5. Combination of OM cross section micrographs (up) and FEA modeled (bottom) foams, with porosities of: (a) 30%, (b) 50% and (c) 70%.

fact that could help in obtaining FEA predictions close to the experimental values.

SEM micrographs were obtained for the analysis of pores at a lower scale, as observed in Fig. 6a and b for the experimental foams with a porosity of 50%. As can be seen, there are not only pores produced by the SHP (already observed in Fig. 5a–c), but also additional porosity associated to the sintering process (interparticle porosity), circled in Fig. 6a and b. It is also important to note that the predominant are the pores of small diameter (lower than 10 μm), as can be observed in Fig. 6b. The analysis of these pores showed that the average D_e is approximately 9 ± 2 μm, and the frequency histogram is not central but moved to the lowest values, being possible to separate two important maxima: high D_e (average = 16 ± 3 μm) pores and small D_e (average = 7 ± 2 μm), in an approximate ratio 1:4.5. This result is similar to the observed for the pores of higher D_e (already analyzed using lower

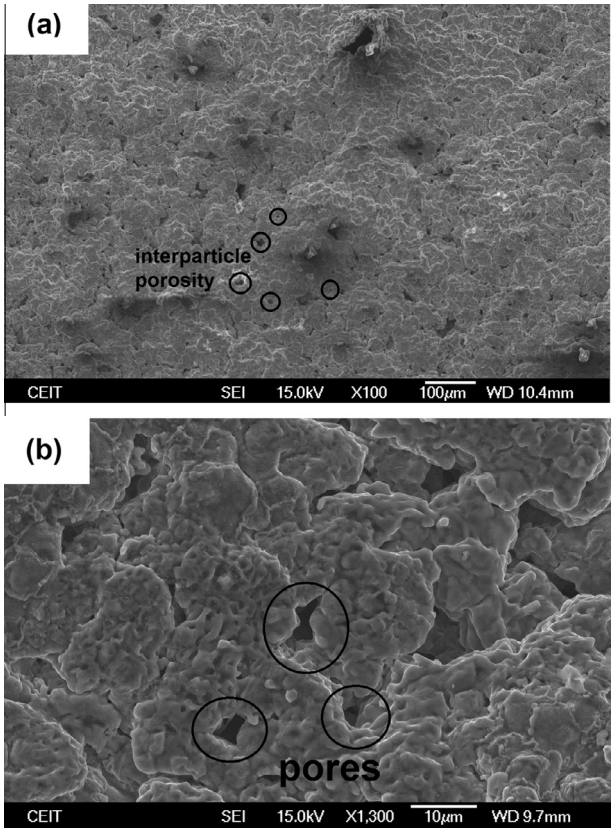

Fig. 6. (a) Scanning Electron Microscopy of the interparticle porosity for the Ti foam with a porosity of 50% and (b) small pores better observed at higher magnifications.

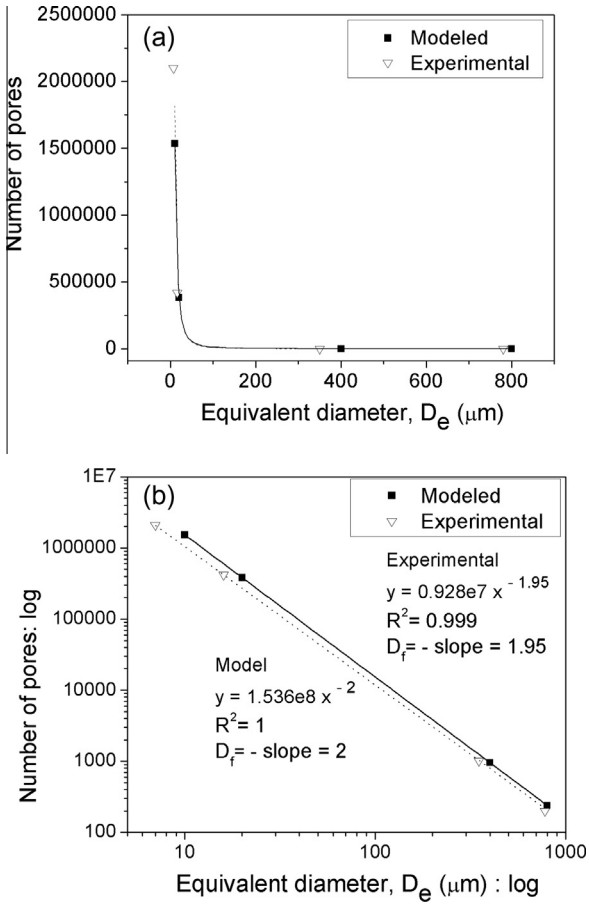

Fig. 7. (a) Relationship between the pore equivalent diameter (D_e) and the number of pores and (b) $Log(D_e)$ versus $Log[N(D_e)]$ indicating the fractal character of the porosity for the foams with a porosity of 50%. The fractal dimensions (D_f) can be observed.

magnifications), with low quantity of big pores and a high quantity of small ones, corresponding to a fractal distribution. These kind of pores have been observed in other works and were expected to appear due to our manufacturing process [8].

Fig. 7a shows the variation of the number of pores (N) against D_e for the model and for the experiments, for a porosity of 50%. For comparison purposes, only four pore sizes were experimentally analyzed (the real microstructure contains dissimilar pores, not only of four homogeneous sizes), corresponding to the used in our model and for the two scales analyzed, already observed in Fig. 5a–c and Fig. 6a and b. The fractal character of the porosity is more clear in the log–log graph of Fig 7b, because points follow a straight line in agreement with a fractal distribution (see Eq. (1)). It is also observed that D_f (corresponding to the slopes) are in good agreement for both, model ($D_f = 2$) and experiments ($D_f = 1.95$). The D_f values agree with other reported fractal size distributions for different features, e.g. pores or grains [27]. A porosity with greater fractal dimension has greater heterogeneity (complexity of pore distribution), so as expected, the modeled porosity is more homogeneous than the real one (due to the presence of pores with different sizes in not exact ratios). These results show the fractal behavior of the porosity in the metallic foams, and the validity of the use of a model that includes pores at different scales. It must be remembered that fractals can be defined as disordered systems that are self similar independent of scale of observation.

4.2. Analysis of the estimations

Examples of the graphical response of the models to the distributed applied loads, for foams with different porosities, can be observed in Fig. 8a–c. As can be seen, the total displacements (compressions) are directly proportional to the porosity. These results were used to determine the Young's moduli (Eqs. (6) and (7)).

FEA estimated results and experimental values for the Young's moduli are compared in Table 1, significantly decreasing with the porosity in both cases. For the experimental foam with a porosity of 30% the Young's modulus is 35.7 GPa, decreasing to 9.3 GPa for the foam with a porosity of 70%; while for the estimations the foam with a porosity of 30% has a Young's modulus of 37.1 GPa, decreasing to 9.3 GPa for the foam with a porosity of 70%. The small relative errors (maximum 11.2%) could be attributed to the fact that the modeled topology is very close to the real one, as already analyzed. Although linear behaviors were obtained for both estimations and experimental results ($E = 59.82 - 0.734P_f$, $R^2 = 0.988$ for estimations; $E = 55.8 - 0.666P_f$, $R^2 = 0.977$ for experiments, where P_f is the porosity and E the Young's modulus), small deviations are expected, as the sudden jump in the relative error for the foams with a porosity of 40%, observed in Table 1. These deviations could be originated, in the case of the estimations, from the intrinsic differences between the models with different porosities, which have random pore arrays (each foam is constituted by dissimilar unit cells), increasing their complexities and the interconnection between pores with the increase in the porosity, as already observed in Fig. 2a–c; and in the case of the experimental results, from a combination of factors including differences in the obtained pore networks and in the Ti matrices (array and bonding of Ti particles; and interparticle porosity). These aspects make very difficult to obtain all the points exactly in the lines of tendency. In the

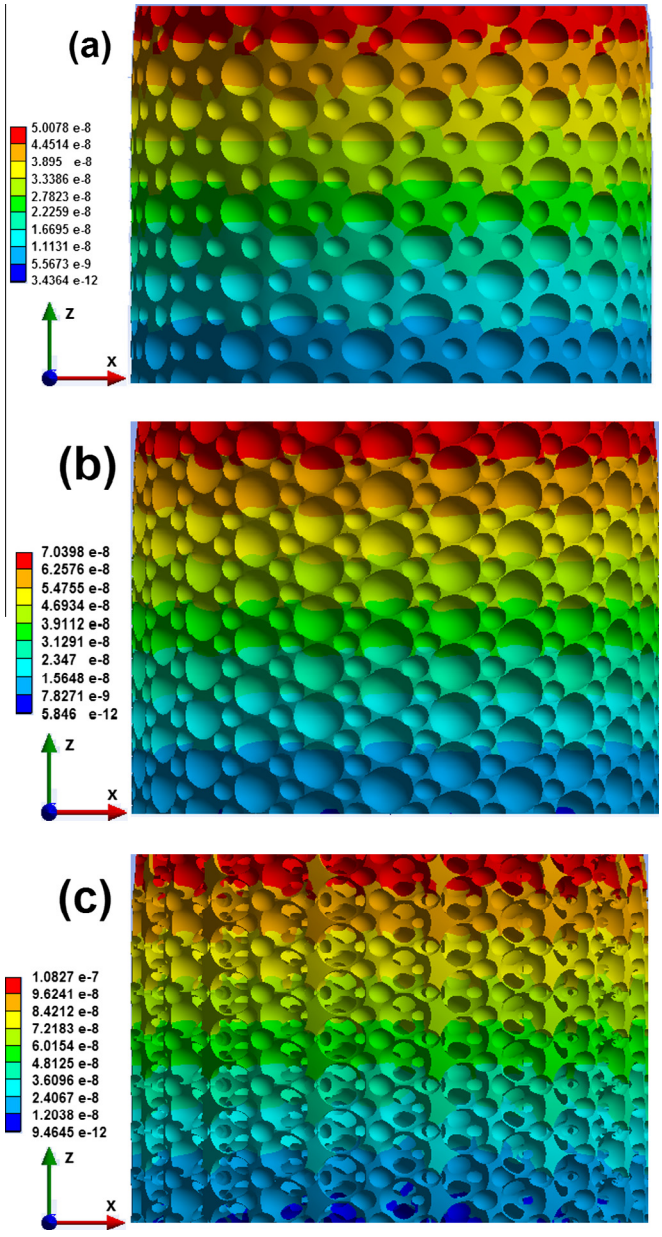

Fig. 8. Axial deformation distributions (in m) of the Ti foam models under compression, for porosities of: (a) 30%, (b) 50% and (c) 70%.

particular case of the foams with a porosity of 40%, coincides that the estimated Young's modulus is above the tendency line, and the experimental Young's modulus is below this line, provoking a higher relative error compared to the other foams. It is important to remark that the experimental yield strengths (YS) and the relative strengths (foam/Ti strengths) also had behaviors similar to the obtained for the Young's moduli, significantly decreasing with the porosity increase. YS were 186.5, 82.7, 68.25, 19.4 and 7.1 MPa, for the foams with porosities of 28%, 38%, 47%, 58% and 68%, respectively. While the relative strength were 0.36, 0.16, 0.10, 0.04 and 0.02, respectively.

Table 1
Estimated and experimental Young's moduli (in GPa) for the materials with different porosities.

	Foam porosity (%)				
	30	40	50	60	70
E, FEA estimated	37.1	31.7	23.6	13.9	9.3
E, experimental	35.7	28.1	25.1	14.3	9.3
Relative error (%)	3.8	11.2	6.6	2.6	0.8

In order to compare the effectiveness of our FEA estimations, three reported models for calculating the elastic modulus of foams were used. The first was the model obtained by Zhu et al. [28]:

$$E_f = \frac{1.009 E_s \rho^2}{1 + 1.514\rho} \tag{8}$$

where E_s is the Young's modulus of the solid material and ρ is the relative density of the foam. Second model is the study by Warren and Kraynik [29]:

$$E_f = \frac{E_s \rho^2 (11 + 4\rho)}{(10 + 31\rho + 4\rho^2)} \tag{9}$$

The last model is the obtained by Nielsen [30]:

$$E_f = E_s \frac{\left(1 - \frac{P}{100}\right)}{1 + \frac{\left(\frac{1}{F} - 1\right)P}{100}} \tag{10}$$

where P is the porosity and F the shape factor. Fig. 9a and b show, respectively, Young's modulus variation with porosity, and the relative errors of these values compared to the experimental results, for FEA estimations and models represented by Eqs. 8–10. It can be clearly observed that the FE model estimations are very close to the experimental results (continuous lines), obtaining the lowest errors. Otherwise, the use of the Nielsen equation over-predicts the

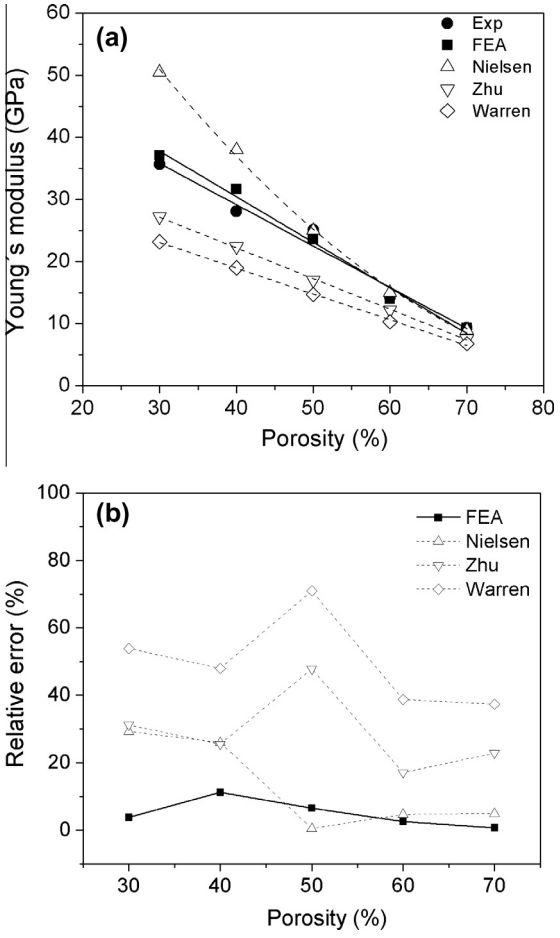

Fig. 9. (a) Compressive Young's modulus variation with porosity and (b) their errors.

Young's moduli, while the Zhu and Warren models under-predict them. These results show the importance of FEA for the study of foams, predicting in an accurate way their compressive behavior. FEA modeling capability allowed to take into account not only the constituent material properties and the porosity percentage, but also the size and shape of the pores, fact that leads to obtain predictions closer to the experimental results. The selection of the foam topology has demonstrated to be an essential variable for obtaining a correct estimation, with relative errors much smaller than the obtained in a previous work [7].

5. Conclusions

After the analysis of the compressive Young's modulus of metallic foams, estimated using new reduced fractal models, and their comparative study for Ti foams with porosities ranging from 30% to 70%, experimentally obtained by means of powder metallurgy, it can be concluded that:

- Fractal models representing more accurately the topology of metallic foams can be obtained from the analysis of the manufacturing process, specifically the features of the space holder.
- The porosity distribution of the experimental Ti foams can be considered as fractal.
- The Young's moduli estimated using the new FE models are in excellent agreement with experiments, decreasing the Young's modulus with porosity. These estimations matched more accurately with the experimental results than the obtained using other reported models, which present relative errors significantly higher, showing the importance of the topology selection and the use of FEA.
- Finally, it was demonstrated that the inclusion of a central hole in the models reduced the computer requirements without affecting the estimations, being a useful modification for the analysis of not only foams but also other materials.

Acknowledgements

L. Pérez acknowledges the financial support from the Chilean Agency CONICYT (FONDECYT project 1140583). I. Alfonso would like to acknowledge the financial support from UNAM PAPIIT TA100114. C. Aguilar would like to acknowledge to Dr. Nieves to supporting in taking FE-SEM images in Centro de Estudios e Investigaciones Técnicas de Gipuskoa, CEIT.

References

[1] G.J. Davies, S. Zhen, Metallic foams: their production, properties and applications, J. Mater. Sci. 18 (1983) 1899, http://dx.doi.org/10.1007/BF00554981.
[2] L.J. Gibson, M.F. Ashby, Cellular Solids: Structure and Properties, second ed., Cambridge University Press, Cambridge UK, 1997.
[3] J. Banhart, H. Eifert, Metal Foams, Verlag MIT Publishing, Bremen, 1997.
[4] J. Banhart, M.F. Ashby, N.A. Fleck, Metal Foams and Porous Metal Structures, Verlag MIT Publishing, Bremen, 1997.
[5] Y. Torres, P. Trueba, J. Pavón, I. Montealegre, J.A. Rodríguez-Ortiz, Designing, processing and characterisation of titanium cylinders with graded porosity: an alternative to stress-shielding solutions, Mater. Design 63 (2014) 316–324, http://dx.doi.org/10.1016/j.matdes.2014.06.012.
[6] J. Banhart, Manufacture, characterisation and application of cellular metals and metal foams, Prog. Mater. Sci. 46 (2001) 559, http://dx.doi.org/10.1016/S0079-6425(00)00002-5.
[7] J.O. Osorio-Hernández, M.A. Suarez, R. Goodall, G.A. Lara-Rodriguez, I. Alfonso, I.A. Figueroa, Manufacturing of open-cell Mg foams by replication process and mechanical properties, Mater. Design 64 (2014) 136–141, http://dx.doi.org/10.1016/j.matdes.2014.07.015.
[8] J.H. Cadena, I. Alfonso, J.H. Ramírez, V. Rodriguez-Iglesias, I.A. Figueroa, C. Aguilar, Improvement of FEA estimations for compression behavior of Mg foams based on experimental observations, Comput. Mater. Sci. 91 (2014) 359–363, http://dx.doi.org/10.1016/j.commatsci.2014.04.065.
[9] N. Jha, D.P. Mondal, J. Dutta Majumdar, A. Badkul, A.K. Jha, A.K. Khare, Highly porous open cell Ti-foam using NaCl as temporary space holder through powder metallurgy route, Mater. Design 47 (2013) 810–819, http://dx.doi.org/10.1016/j.matdes.2013.01.005.
[10] Y. Chino, D.C. Dunand, Creating aligned, elongated pores in Titanium foams by swaging of preforms with ductile Space-Holder, Adv. Eng. Mater. 11 (2008) 52–55, http://dx.doi.org/10.1002/adem.200800232.
[11] J. Jakubowicz, G. Adamek, M. Dewidar, Titanium foam made with saccharose as a space holder, J. Porous Mat. 20 (2013) 1137–1141, http://dx.doi.org/10.1007/s10934-013-9696-0.
[12] F. Mat Noor, M.I.M. Zain, K.R. Jamaludin, R. Hussin, Z. Kamdi, A. Ismail, S. Ahmad, H. Taib, Potassium bromide as space holder for titanium foam preparation, Appl. Mech. Mater. 465–466 (2014) 922–926, http://dx.doi.org/10.4028/www.scientific.net/AMM.465-466.922.
[13] Y. Torres, J.A. Rodríguez, S. Arias, M. Echeverry, S. Robledo, V. Amigó, J.J. Pavón, Processing, characterization and biological testing of porous titanium obtained by space-holder technique, J. Mater. Sci. 47 (2012) 6565–6576, http://dx.doi.org/10.1007/s10853-012-6586-9.
[14] Y. Torres, J. Pavón, J.A. Rodríguez, Processing and characterization of porous titanium for implants by using NaCl as space holder, J. Mater. Proc. Technol. 212 (2012) 1061–1069, http://dx.doi.org/10.1016/j.jmatprotec.2011.12.015.
[15] Y. Torres, S. Lascano, J. Bris, J. Pavón, J.A. Rodriguez, Development of porous titanium for biomedical applications: a comparison between loose sintering and space-holder techniques, Mater. Sci. Eng. C 37 (2014) 148–155, http://dx.doi.org/10.1016/j.msec.2013.11.036.
[16] P.R. Marur, Numerical estimation of effective elastic moduli of syntactic foams, Finite Elem. Anal. Des. 46 (2010) 1001–1007, http://dx.doi.org/10.1016/j.finel.2010.07.006.
[17] R. Jhaver, H. Tippur, Processing, compression response and finite element modeling of syntactic foam based interpenetrating phase composite (IPC), Mater. Sci. Eng. A 499 (2009) 507–517, http://dx.doi.org/10.1016/j.msea.2008.09.042.
[18] H.W. Song, Q.J. He, Mechanics of metallic foams: a fractal approach, in: Advances in Heterogeneous Material Mechanics, 2nd International Conference on Heterogeneous Material Mechanics, June 3–8, 2008, Huangshan, China, pp. 870–874.
[19] X. Zhang, G. Jia, H. Huang, Numerical investigation of aluminum foam shield based on fractal theory and node-separation FEM, Chinese J. Aeronaut. 24 (2011) 734–740, http://dx.doi.org/10.1016/S1000-9361(11)60086-1.
[20] B.B. Mandelbrot, D.E. Passoja, A.J. Paullay, Fractal character of fracture surface of metals, Nature 308 (1984) 721–722, http://dx.doi.org/10.1038/308721a0.
[21] D. Perugini, G. Poli, Tourmaline nodules from Capo Bianco aplite (Elba Island, Italy): an example of diffusion limited aggregation growth in a magmatic system, Contrib. Mineral Petr. 153 (2007) 493–508, http://dx.doi.org/10.1007/s00410-006-0167-3.
[22] Best Samuel, Development and Implementation of a Dual-Porosity Pore Network Structure using X-ray Computed Tomography for Pore Network Modeling Purposes, Thesis Master of Science in Civil Engineering, Louisiana State University, 2011.
[23] R. Peng, Y. Yang, Y. Ju, L. Mao, Y. Yang, Computation of fractal dimension of rock pores based on gray CT images, Chinese Sci. Bull. 56 (2011) 3346–3357, http://dx.doi.org/10.1007/s11434-011-4683-9.
[24] E. Ogris, H. Luchinger, P.J. Uggowitzer, Silicon spheroidization treatment of thixoformed Al–Si–Mg alloys, Mater. Sci. Forum. 396–402 (2002) 149–154, http://dx.doi.org/10.4028/www.scientific.net/MSF.396-402.149.
[25] Y.Y. Zhao, D.X. Sun, A novel sintering-dissolution process for manufacturing Al foams, Scripta Mater 144 (2000) 105, http://dx.doi.org/10.1016/S1359-6462(00)00548-0.
[26] M. Kırca, A. Gul, E. Ekinci, F. Yardım, A. Mugan, Computational modeling of micro-cellular carbon foams, Finite Elem. Anal. Des. 44 (2007) 45–52, http://dx.doi.org/10.1016/j.finel.2007.08.008.
[27] S.K. Sebsadji, K. Chouicha, Determining periodic representative volumes of concrete mixtures based on the fractal analysis, Int. J. Solids Struct. 49 (2012) 2941–2950, http://dx.doi.org/10.1016/j.ijsolstr.2012.05.017.
[28] H.X. Zhu, N.J. Mills, J.F. Knott, Analysis of the high strain compression of open cell foams, J. Mech. Phys. Solids 45 (1997) 1875–1904, http://dx.doi.org/10.1016/S0022-5096(97)00027-6.
[29] W.E. Warren, A.M. Kraynik, The linear elastic properties of open cell foams, J. Appl. Mech. 55 (1988) 341–346, http://dx.doi.org/10.1115/1.3173680.
[30] L.F. Nielsen, Elasticity and damping of porous materials and impregnated materials, J. Am. Ceram. Soc. 67 (1984) 93–98, http://dx.doi.org/10.1111/j.1151-2916.1984.tb09622.x.